第 34 卷第 11 期
2018 年 11 月

无 机 化 学 学 报
CHINESE JOURNAL OF INORGANIC CHEMISTRY

Vol.34 No.11
2088-2096

锰活性物质负载 Ti 掺杂 SiO_2 纳米管复合催化剂的制备及其 NH_3-SCR 反应活性

叶永洲[1] 沈 飞[1] 王红宁[1] 陈若愚*,[1] 孙 林*,[2,3]

([1]常州大学石油化工学院,常州 213164)

([2]江苏高校生态建材与环保装备协同创新中心;盐城工学院化学化工学院,盐城 224051)

([3]南京大学配位化学国家重点实验室,南京 210023)

摘要:利用溶胶–凝胶法以及共缩聚反应合成得到了新型的 Ti 掺杂 SiO_2 纳米管(TiSNTs)。然后,利用共沉淀的方法在该催化剂上负载了不同 Mn 含量的 Mn/TiSNTs 复合催化剂。当 Si 与 Ti 的物质的量之比超过 5 时,可以看到形成了很清楚的蠕虫状形貌。NH_3-TPD(氨气程序升温脱附)测试结果显示掺杂到 SiO_2 骨架中的 Ti 极大增强了催化剂的酸性位点而且提高了 NH_3 在催化剂表面的吸附量和氨选择性催化还原(NH_3-SCR)的活性。同时,H_2-TPR(氢气程序升温还原)测试结果显示 Ti 掺杂增强了催化剂的氧化还原能力和储氧容量。NH_3 还原 NO_x 的 SCR 结果说明当 Si 与 Ti 的物质的量之比为 10 的时候,Mn/Ti(10)SNT 催化剂显示了优异的催化活性,在温度范围为 135~325 ℃时 NO 转化率超过 90%。

关键词:异相催化;负载型催化剂;二氧化硅;纳米管;溶胶–凝胶过程

中图分类号:O614.41+1;O613.72;O643.36 **文献标识码**:A **文章编号**:1001-4861(2018)11-2088-09

DOI:10.11862/CJIC.2018.260

Preparation of Titania Doped SiO_2 Nanotube Composites with Manganese Loadings for NH_3-SCR Applications

YE Yong-Zhou[1] SHEN Fei[1] WANG Hong-Ning[1] CHEN Ruo-Yu*,[1] SUN Lin*,[2,3]

([1]*School of Petrochemical Engineering, Changzhou University, Changzhou, Jiangsu* 213164, *China*)

([2]*Jiangsu Collaborative Innovation Center for Ecological Building Materials and Environmental Protection Equipments; School of Chemistry and Chemical Engineering, Yancheng Institute of Technology, Yancheng, Jiangsu* 224051, *China*)

([3]*State Key Laboratory of Coordination Chemistry, Nanjing University, Nanjing* 210023, *China*)

Abstract: Ti-containing SiO_2 nanotubes (TiSNTs) were firstly synthesized via a sol-gel and co-polycondensation method. After that, a family of Mn doped TiSNTs (Mn/TiSNTs) catalysts with various Mn loading were prepared via the co-precipitation method. When Si/Ti molar ratio was more than 5, a worm-like tubular morphology was clearly observed. The NH_3-TPD (NH_3-temperature programmed desorption) results show that the Ti doping into the skeleton of the silica nanotubes greatly enhanced the acidic sites of the catalyst and promoted the adsorption and NH_3-SCR (selective catalytic reduction) activation on the surface of the catalyst. Meanwhile, the results of H_2-TPR (H_2-temperature programmed reduction) also show that Ti doping enhanced the redox ability of the catalyst and the capacity of oxygen storage. Moreover, the doped Mn species was beneficial for reducing the reaction temperature. The results of SCR of NO_x with NH_3 show the catalyst with Si/Ti molar ratios of 10 (Mn/Ti(10)SNT) exhibited significant catalytic activity, and the NO conversion rate remained over 90% in the reactive temperature range of 135 to 325 ℃.

Keywords: heterogeneous catalysis; supported catalysts; silicates; nanotubes; sol-gel processes

收稿日期:2018-07-08。收修改稿日期:2018-09-11。

国家自然科学基金(No.21571024,21101017/B0107),江苏省自然科学基金(No.BK20181056),江苏省普通高校研究生科研创新计划(No.SJZZ15_0142)和配位化学国家重点实验室开发课题(No.SKLCC1802)资助。

*通信联系人。E-mail:cxdcry@163.com,sunlin1987@126.com

0 Introduction

Nitrogen oxides (NO_x) emitted from automobile exhaust or chemical manufacturing industrials evoke serious environmental problems, including acid rain, photochemical smog, and greenhouse effects. The selective catalytic reduction (SCR) of NO_x with ammonia (NH_3) is the most effective means to remove NO_x species[1-2]. Transition metal (Fe, Mn, Co, Cr and Ni), zeolite-based catalysts have been developed to solve this problem[3-4]. In particular, Mn-based zeolite catalysts exhibit excellent NO removal efficiency because of their variable valence state, strong redox capability and abundant acidic sites. Wang et al.[5] reported that composite SCR catalysts composed of MnO_x and multi-walled carbon nanotube (MWCNT) demonstrated excellent activity, and the NO_x conversion rate was more than 90% at low temperature of 190 ℃. Lou et al.[6] reported that Mn/ZSM-5 catalysts exhibited comparable SCR reaction activity in the low-temperature range of 170~350 ℃. Yu et al.[7] found that the MnSAPO-34 molecular sieve catalysts prepared at 550 ℃ exhibited the best SCR activity with the NO conversion nearly as high as l00%, and the catalytic activity was rapidly improved at 250~300 ℃.

It is worth noting that different catalyst carriers also have important effects on SCR activity. Al_2O_3 have been widely studied as low-temperature SCR catalyst supports[8-9] because the surface of the Al_2O_3 carrier is modified with many hydroxyl groups, thus are beneficial for the oxidation of NO into NO_2 and maintaining the reaction between nitrogen oxides and ammonia at low temperatures. For example, Xie et al.[10] reported that the NO conversion rate reached around 80% at 200 ℃ over CuO/Al_2O_3 catalysts. Activated carbon is another widely used carrier for the SCR catalyst because of the strong adsorption capability for NO molecules at low temperatures. The research results have confirmed that activated carbon combined with CuO exhibited high SCR activity at low temperature of 200 ℃[11]. In addition, the abundant Lewis acid sites on the surface of TiO_2 are beneficial for the adsorption and activation of ammonia during the SCR reaction. Therefore, TiO_2 can also be employed as carriers for the SCR catalyst.

Kato et al.[12] reported that the removal efficiency of NO could reach more than 60% from 250 to 450 ℃ for the Fe_2O_3/TiO_2 composite catalysts. Recent studies have also showed that Ti-SBA-15, Ti-MCM-41, TS-1 and Ti-grafted SiO_2 can provide abundant acid sites due to the incorporation of titanium[13-15].

SiO_2 nanotubes with high surface area are considered as ideal supports for the dispersion of the active components of the SCR catalyst and enrichment of target gases. Moreover, it should be indicated that if the titanium can be incorporated into the skeleton of SiO_2 nanotubes, the strong redox capability and large oxygen storage capacity can be achieved within surface concentration. In this study, Mn and Ti co-doped SiO_2 nanotubes (Mn/TiSNTs) were rationally designed and synthesized via assembling of several methods such as co-polycondensation and co-precipitation. The obtained Mn/TiSNTs catalysts exhibited significant SCR activity under low reaction temperatures due to the synergistic effect of different active components and SiO_2 nanotube supports with high surface area.

1 Experimental

1.1 Preparation of Mn/TiSNT catalysts

The Ti-containing SiO_2 nanotubes (TiSNT) with different Si/Ti molar ratios were synthesized via a sol-gel method. The 1.00 g of Pluronic F127 was dissolved in 60 mL of 2 $mol \cdot L^{-1}$ HCl in a glass container with magnetic stirring followed by 2.8 g of tetraethyl orthosilicate. Tetrabutyl titanate was dissolved into 3 mL of toluene, and the resulting solution was slowly added into this solution. The solution was stirred at 250 $r \cdot min^{-1}$ and 11 ℃ for 24 h in a covered container. The gel was transferred into Teflon-lined autoclaves and heated to 100 ℃ for 24 h. The product was filtered, washed and dried in a vacuum oven at 55 ℃. The as-synthesized product was calcined at 350 ℃ in air for 5 h. The synthesized samples were hereafter denoted as Ti(x)SNT where x represents the Si/Ti molar ratio.

According to the previous research, the Mn/TiSNT catalyst with optimized 5.5%(*w*/*w*) Mn loading shows the largest specific surface area of 430 $m^2 \cdot g^{-1}$ [16]. The Mn/Ti(*x*)SNT catalysts were similarly prepared by precipitation with NH_3. A specific proportion of the Ti(*x*)SNT sample was ion exchanged with appropriate amounts of manganese acetate under magnetic stirring at room temperature for 24 h. Ammonia was slowly added to adjust the pH value to 11. The solution was then filtered, washed with deionized water and dried at 100 ℃ overnight followed by calcination at 350 ℃ for 2 h. The synthesized catalyst samples were hereafter denoted as Mn/Ti(*x*)SNT, where *x* represents the Si/Ti molar ratio.

1.2 Characterizations

XRD patterns of the products were obtained using a Rigaku D/MAX2500 diffractometer with a Cu *Kα* radiation source (λ=0.154 nm), a tube voltage of 40 kV, and a tube current of 100 mA in the 2θ range of 5°~70° with a scanning rate of 3°·min^{-1}. TEM images were obtained by using JEM-2100 (with operation voltage of 200 kV). The N_2 adsorption-desorption isotherms were determined using a Quantachrome Autosorb-iQ2-MP N_2 adsorption instrument. All of the samples were held in a vacuum at 300 ℃ for 5 h prior to measurement to ensure the elimination of water and other superfluous species. The micropore volume was measured via a *t*-plot method. The specific surface area was calculated using the Brunauer-Emmett-Teller (BET) method. UV-Raman spectroscopy was conducted on a Thermo Fisher Scientific DXR Raman spectrometer. A laser line at 325 nm was employed as the excitation source. The UV-Vis DRS spectra were obtained on a Shimadzu UV-2450 UV-Vis spectrophotometer from 200 to 800 nm. The atomic concentrations on the sample surfaces were evaluated using XPS on a Kratos Analytical AXIS Ultra DLD spectrometer. The binding energy of the C1*s* peak (284.8 eV) was used as an internal standard. The TPD of NH_3 (NH_3-TPD) determined the number of different acid sites and their strengths for the catalysts using a Micromeritics AutoChem 2920 automated catalyst characterization system.

Prior to test, ~30 mg of the catalyst was pretreated with high-purity N_2 at 40 mL·min^{-1} and 500 ℃ for 60 min. Then, physical absorbed ammonium was removed via helium under equivalent conditions. The TPD operation was conducted next a heating rate of 10 ℃·min^{-1} from 100 to 800 ℃. The amount of desorbed NH_3 was determined via a thermal conductivity detector (TCD). The TPR runs were carried out with a linear rate (10 ℃·min^{-1}) in pure N_2 containing 5%(*V*/*V*) H_2 at a flow rate of 30 mL·min^{-1}.

1.3 NH_3-SCR activity testing

The catalytic activities of the Mn/Ti(*x*)SNT samples were investigated using a custom-made fixed bed. For each sample, about 500 mg of the catalyst was placed in a quartz tube reactor with 1 cm in diameter. This was mixed with quartz sand to ensure the smooth passage of the reaction gas through the reactor. The reaction gas was composed of 8%(*V*/*V*) O_2, 600 mg·L^{-1} NO, 600 mg·L^{-1} NH_3 and 5%(*V*/*V*) H_2O. The balance was N_2, 300 mL·min^{-1} total flow rate and a gas hourly space velocity (GHSV) of 36 000 h^{-1} was employed. The concentration of NO in the reactors outlet gas was analyzed via a gas analyzer (FGA-4100, Guangdong Foshan Analytical Instrument Co., Ltd.).

The NO conversion (Eq.(**1**)) and N_2 selectivity (Eq.(**2**)) were respectively calculated as follows:

$$\text{NO conversion}=(C_{NO}^{in}-C_{NO}^{out})/C_{NO}^{in}\times 100\% \quad (\mathbf{1})$$

$$N_2 \text{ selectivity}=C_{N_2}^{out}/(C_{NO}^{in}-C_{NO}^{out})\times 100\% \quad (\mathbf{2})$$

Where C_{NO}^{in} and C_{NO}^{out} are the respective concentrations of NO at the inlet and the outlet of the reactor, $C_{N_2}^{out}$ is the concentration of N_2 at the outlet.

2 Results and discussion

2.1 Morphology and composition analysis

Fig.1 shows TEM images of Ti-containing SNT samples with different Si/Ti molar ratios. At relatively high Si/Ti molar ratios such as Ti(20)SNT, Ti(15)SNT and Ti(10)SNT, the worm-like tubular morphology was clearly observed, which are illustrated in Fig.1(A~C). Meanwhile, TEM images clearly confirmed the hollow structure of the worm-like rods. However, when the

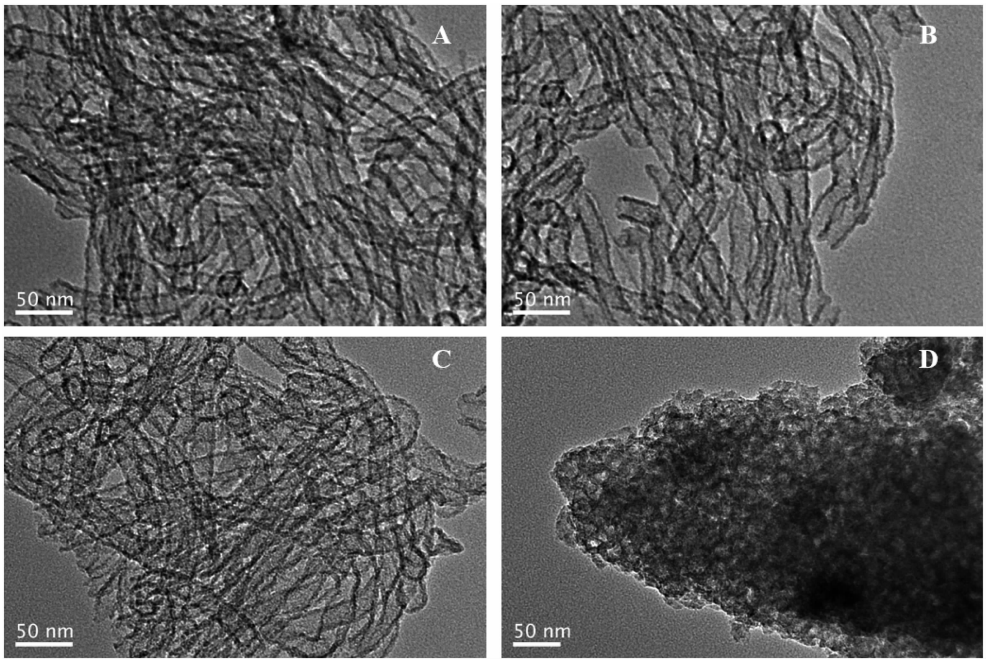

(A) Ti(20)SNT; (B) Ti(15)SNT; (C) Ti(10)SNT; (D) Ti(5)SNT

Fig.1　TEM images of Ti-containing SNT with different Si/Ti molar ratios

molar ratio of Si/Ti was reduced to 5(Ti(5)SNT), the worm-like tubular morphology disappeared, in other words, the tubular morphology of Ti(5)SNT was destroyed, as shown in Fig.1D. This is mainly due to the higher content of titanium precursor and fast hydrolysis rate of titanium precursor, which significantly affect the assembly of the template and the SiO_2 precursor resulting in the formation of tubular structures.

Moreover, the elemental composition of Mn/Ti(x) SNT samples was measured by a Varian Vista-AX inductively coupled plasma optical emission spectrometer (ICP-OES). The Si/Ti test ratio (n_{Si}/n_{Ti}) of Ti-containing SNT was close to the theoretical value, the results are shown in Table 1.

Table 1　Element composition of Ti-containing SNT with different Si/Ti molar ratios

Sample	w_{Si}/w_{Ti}	Mass fraction of Mn / %	n_{Si}/n_{Ti}
Ti(20)SNT	10.78	5.5	18
Ti(15)SNT	7.60	5.7	13
Ti(10)SNT	5.02	5.5	9
Ti(5)SNT	2.44	5.4	4

2.2　XRD patterns

XRD patterns of Ti-containing SNT samples with different Si/Ti molar ratios are shown in Fig.2. For Ti-containing SNT, an intense diffraction peak located at 23.4° is clearly observed, and the peak can be attributed to the characteristic peaks of amorphous silica. For Ti(5)SNT, two weak diffraction peaks were located at 25.2° and 27.2°. Both peaks could be attributed to anatase TiO_2 phase. This was possibly because the hydrolysis rate of the titanium precursor was faster and played a leading role resulting in the formation of TiO_2 nanoparticles. The Si source could not form a tubular structure. When Si/Ti molar ratio was more than 5, the anatase phase was not detected

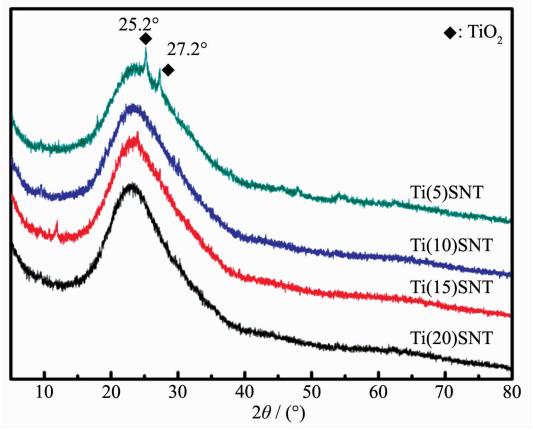

Fig.2　XRD patterns of Ti-containing SNT with different Si/Ti molar ratios

in the XRD patterns. It may be speculated that the relatively small amount of titanium could not be detected due to the small particles of titanium. The excessive amount of the titanium precursor will affect the formation of SiO_2 hollow nanotube structures.

2.3 UV-Vis DRS analysis

UV-Vis DRS spectroscopy was used to understand the nature and coordination of the Ti species in the Ti-containing SNT. UV-Vis DRS spectroscopy of the Ti-containing SNT samples with different Si/Ti molar ratios are shown in Fig.3. A strong absorbance band at 220 nm was observed on Ti(20)SNT, Ti(15)SNT and Ti(10)SNT samples. These were attributed to isolated framework titanium in tetrahedral coordination. The Ti atoms likely substitute for Si atoms in the skeleton of SNT structures with the formation of a Ti-O-Si-Ti band[17-18]. No absorbance band was observed in the SNT sample. A strong absorbnce band at 310~340 nm was observed for the Ti(5)SNT sample, which indicated the presence of polytitanium $(Ti\text{-}O\text{-}Ti)_n$ clusters[19], implying the formation of a crystalline TiO_2 phase. No absorbance band was seen at 220 nm in UV-Vis DRS spectroscopy. The Ti atoms do not exist in the skeleton of the SNT structure. In contrast, its peak is too weak to be masked. TEM images do not show a tubular morphology, thus we suspect that the hydrolysis rate of the titanium precursor is faster, which will result in the formation of polytitanium $(Ti\text{-}O\text{-}Ti)_n$ clusters.

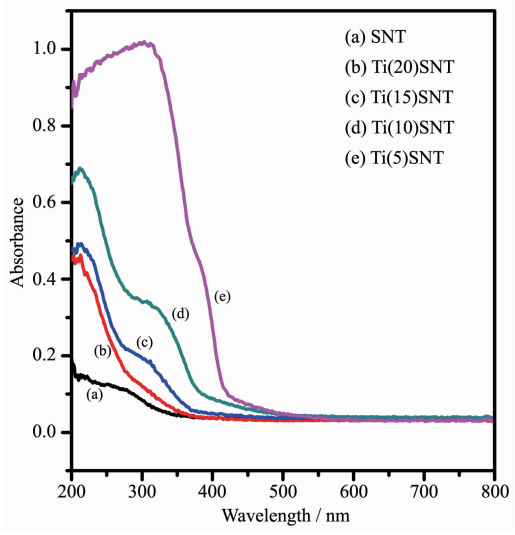

Fig.3 UV-Vis DRS spectra of Ti-containing SNT with different Si/Ti molar ratios

Based on these characterization results, we synthesized Ti-containing silicon nanotubes with defined hollow tubular structures. The addition of titanium affects the formation of the tubular structures. With Si/Ti molar ratio was fixed over 5 (as Ti(20)SNT, Ti(15)SNT and Ti(10)SNT samples), the Ti species embedded into the framework of SNT and were served as Ti atoms in tetrahedral coordination. When the molar ratio of Si/Ti was 5, the Ti species existed as polytitanium $(Ti\text{-}O\text{-}Ti)_n$ clusters, which distorted the tetrahedral environment.

2.4 N_2 adsorption-desorption

Fig.4a shows the N_2 adsorption-desorption isotherms of Mn/TiSNT catalyst samples. It is shown that all of the Mn/TiSNT samples exhibited classical Ⅳ-type isotherms with an obvious H4 hysteresis loop as defined by IUPAC. This indicates that a mesopore structure existed in these catalysts. There are two capillary condensation steps in the adsorption isotherms indicating that the catalysts had two types of mesopores. The hysteresis loop at relatively low pressure corresponds to the inner void of the hollow nanospheres, and the hysteresis loop in the relatively high pressure is ascribed to the interparticle void formed from nanosphere packing. Fig.4b exhibits the narrow mesopore distributions of Mn/TiSNT samples, and the pore diameter increased with the decreasement of Ti. Table 2 shows the BET surface area, pore volume and average pore diameter of Mn/TiSNT catalysts. The BET surface area, pore volume and average pore diameter of catalysts decreased with an increasing amount of doped titanium. When the Si/Ti molar ratios of the Mn/TiSNT catalysts were over 5, the BET surface area, pore volume and average pore

Table 2 Textural properties of Mn/Ti(x)SNT catalysts

Catalyst	BET surface area / ($m^2 \cdot g^{-1}$)	Pore volume / ($cm^3 \cdot g^{-1}$)	Average pore diameter / nm
Mn/Ti(20)SNT	460	0.011 0	11.4
Mn/Ti(15)SNT	450	0.010 1	10.2
Mn/Ti(10)SNT	435	0.009 6	9.3
Mn/Ti(5)SNT	286	0.007 3	8.0

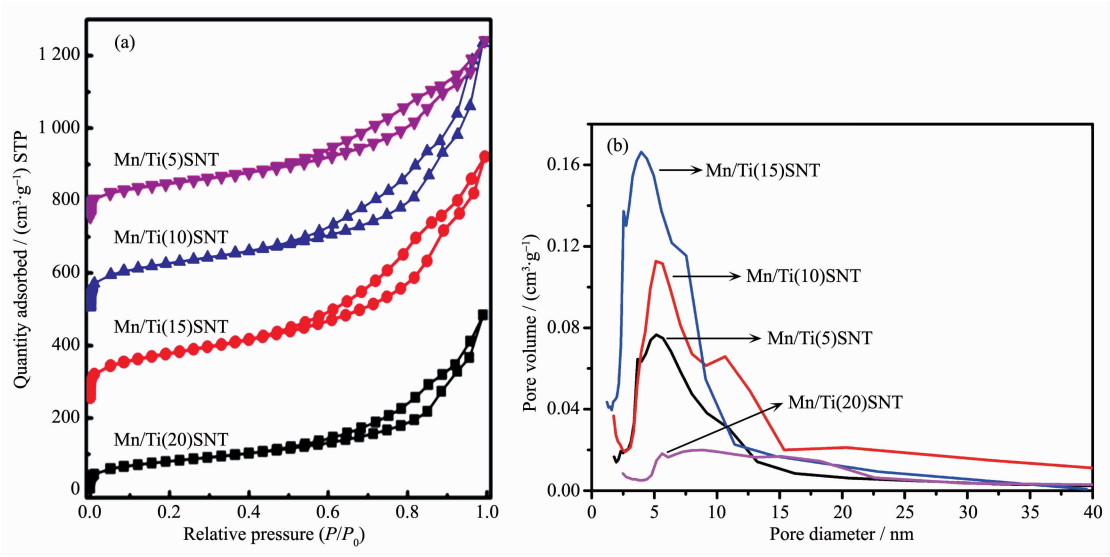

Fig.4　(a) Nitrogen adsorption-desorption isotherms of Mn/TiSNT catalysts with different Si/Ti molar ratios; (b) Pore distributions of Mn/TiSNT catalysts

diameter of the Mn/TiSNT catalysts decreased slightly with increasing amounts of doped titanium. When the Si/Ti molar ratio of the Mn/TiSNT catalyst was 5, the surface area decreased dramatically from 435 to 286 $m^2 \cdot g^{-1}$ due to the morphology transformation of hollow SiO_2 nanotubes.

2.5　XPS results

The catalysts are characterized by XPS to evaluate the oxidation state of Mn and to estimate the concentrations of Mn on the surface of the Mn/TiSNT catalysts. Fig.5 presents the Mn2*p* XPS spectra of the Mn/Ti(20)SNT and Mn/Ti(10)SNT catalysts, which consist of asymmetrical Mn2$p_{3/2}$ and Mn2$p_{1/2}$ vibrational

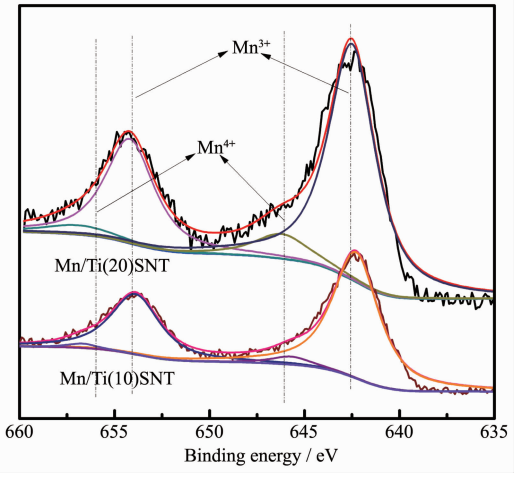

Fig.5　Mn2*p* XPS spectra of Mn/TiSNT catalyst with different Si/Ti molar ratios

peaks with binding energies of about 642.3 and 653.8 eV, respectively. Deconvolution fitting of the Mn2$p_{3/2}$ and Mn2$p_{1/2}$ peaks yields four distinct peaks centered at 642.1, 653.4, 643.8 and 656.1 eV. These were slightly shifted relative to standard literature values.

The asymmetric Mn2$p_{3/2}$ peak indicated the presence of a mixed-valence manganese species. The Mn2$p_{3/2}$ peaks near 656.1 eV and the Mn2$p_{1/2}$ peaks near 643.8 eV were assigned to Mn^{4+} [20-21] proving the presence of the MnO_2 species on the catalyst surface. XRD patterns show no MnO_2 crystals on the catalysts. The Mn2$p_{3/2}$ and Mn2$p_{1/2}$ peaks at approximately 653.4 and 642.1 eV were assigned to Mn^{3+}[22-23], proving the presence of the Mn_2O_3 species on the catalyst surface.

The O1*s* core level peak of the Mn/Ti(20)SNT and Mn/Ti(10)SNT catalysts are shown in Fig.6. The O1*s* spectra of all catalysts show two distinct peaks with binding energies of 532.3~534.1 eV and 529.1~530.2 eV, which were assigned to the weakly surface-adsorbed oxygen ions ($O_{adsorbed}$) and the lattice oxygen ($O_{lattice}$), respectively (The atom ratios of $O_{lattice}$ to $O_{adsorbed}$ was shown in Table 3)[24-25]. The introduction of the Ti species to the silicon nanotubes results in major changes in the content of surface-adsorbed oxygen. It is obvious that the intensity of surface-adsorbed oxygen increased with the decreasing Si/Ti molar ratio. This is because Ti incorporation leads to charge

Table 3 Atom ratios of $O_{lattice}$ to $O_{adsorbed}$

Sample	Mn/Ti(5)SNT	Mn/Ti(10)SNT	Mn/Ti(15)SNT	Mn/Ti(20)SNT
$n_{O(lattice)}$ / $n_{O(adsorbed)}$	6.11%	45.4%	7.31%	0.94%

imbalance, and this leads to the formation of vacancies and unsaturated chemical bonds on the catalyst surface.

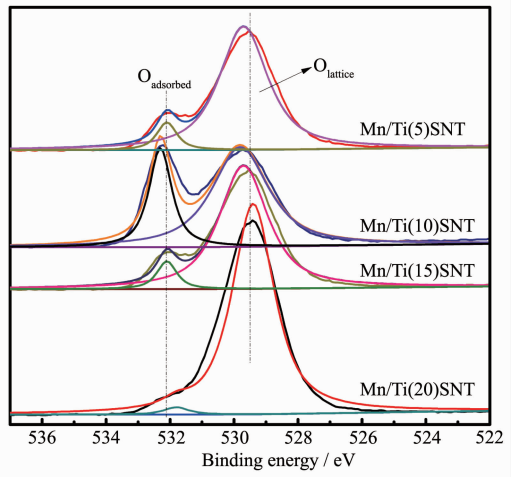

Fig.6 O1*s* XPS spectra of Mn/TiSNT catalysts with different Si/Ti molar ratios

It is well known that surface-adsorbed oxygen plays an important role in NH_3-SCR, and this can promote the oxidation of NO to NO_2. Therefore, an increase in surface-adsorbed oxygen on the catalyst surface has a positive effect on the SCR reaction. When the Si/Ti molar ratio was 5, the amount of surface-adsorbed oxygen decreased sharply. This may be related to its morphology and the formation of polytitanium $(Ti\text{-}O\text{-}Ti)_n$ clusters that decreased the catalytic activity of Mn/Ti(5)SNT catalysts.

2.6 SCR activity

The NO conversion rates for the SCR reaction were evaluated on Mn/TiSNT catalysts with different Si/Ti molar ratios between 50 and 350 ℃ (Fig.7A). The Si/Ti molar ratio impressed an obvious influence on the catalytic performance of the Mn/TiSNT catalyst. As the reaction temperature increases, the NO conversion rate of all Mn/TiSNT catalysts increased initially, then they reached the highest conversion rate and maintained at this level for a while. The conversion rates subsequently decreased with an increase in the operating temperature. Fig.7B also shows the N_2 selectivity for these catalysts, all of which exhibited high selectivity through the entire temperature range.

The Mn/Ti(10)SNT catalysts possess the highest SCR activity at low temperature amongest all catalysts studied. The Mn/Ti(10)SNT catalyst endows NO conversion rates as high as 90% at 135 ℃, and shows excellent catalytic activity from 135~325 ℃ (NO conversion over 90%). When the amount of titanium doping is excessive, the catalytic activity of the Mn/Ti (5)SNT catalyst was drastically decreased. The NO_x removal activity of the Mn/TiSNT catalysts follows the order of Ti(10)SNT>Ti(15)SNT>Ti(20)SNT>Ti(5)SNT. These results clearly suggest that higher titanium doping decreased the deNO_x activity of Mn/TiSNT catalysts.

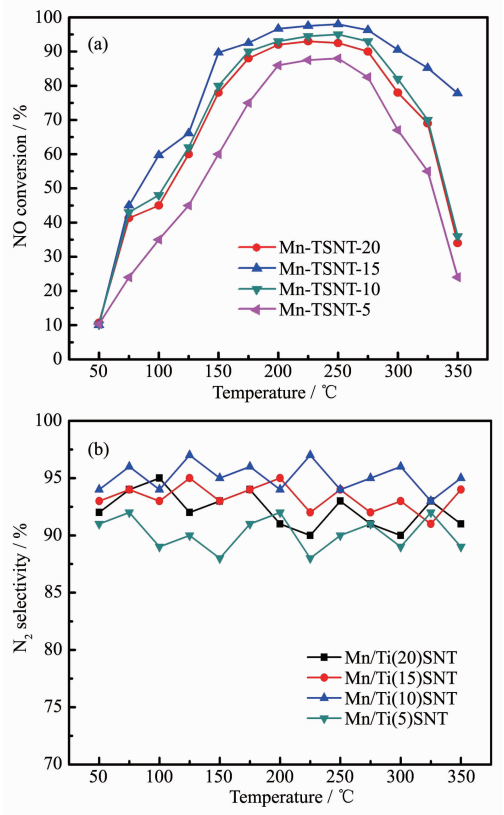

Fig.7 (A) Catalytic performance for SCR of NO with ammonia and (B) N_2 selectivity of Mn/TiSNT catalysts with different Si/Ti molar ratios as a function of temperature

2.7 NH_3-TPD and H_2-TPR analysis

NH_3-TPD was used to determine the catalysts strength and amount of different acid sites-the acidity of the catalyst is beneficial for the adsorption and activation of NH_3. The NH_3-TPD curves for all samples contained three desorption peaks (Fig.8). The peaks from 100 to 250 ℃ were attributed to ammonium species adsorbed at weak Lewis acid sites or weakly adsorbed NH_3[26]. The peaks from 250 to 400 ℃ were assigned to ammonia adsorbed on strong Brnsted acid sites[27]. The peaks from 400 to 600 ℃ were due to strong Brnsted acid sites formed by the interaction of Brnsted acid sites with extra-framework titanium species[28-29].

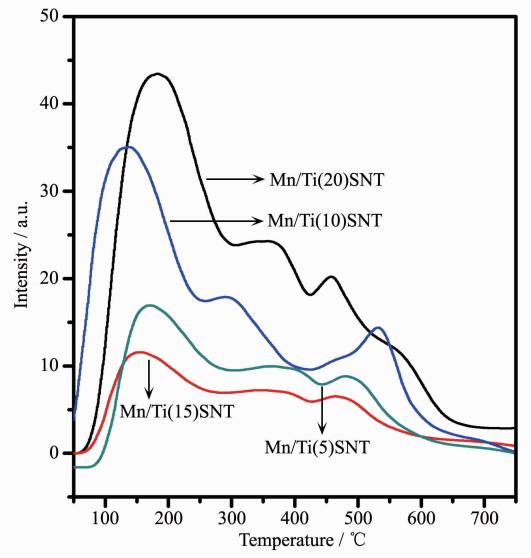

Fig.8 NH_3-TPD curves of Mn/TiSNT catalysts with different Si/Ti molar ratios

For the Mn/Ti(10)SNT catalyst, the intensity of the peak in the temperature range of 400~600 ℃ was significantly higher than other catalysts with different Si/Ti molar ratios. This indicates that when the Si/Ti molar ratio was 10, the amount of acid sites of the catalyst increase-especially the strong acid sites on the catalyst surface. This promotes the adsorption and activation of NH_3 on the surface of the catalyst. Therefore, the SCR activity of the catalyst was improved at low-temperature regions.

The H_2-TPR profiles for Mn/TiSNT catalysts with different Si/Ti molar ratios are presented in Fig.9. The redox properties of the catalysts are affected by the amount of doped titanium. The Mn/TiSNT catalyst exhibited a broad reduction peak from 200 to 400 ℃; this corresponded to the following successive reduction process: $MnO_2 \rightarrow Mn_2O_3 \rightarrow Mn_3O_4 \rightarrow MnO$[30-31]. The reduction peak of the Mn/TiSNT catalysts increased with an increasing amount of doped titanium. The results show that Ti doping could enhance the redox ability and oxygen storage capacity of the Mn/TiSNT catalyst. With an increasing amount of doped titanium, the reduction peak gradually shifted to a higher temperature. This indicated that the redox reaction of the catalyst occurred at a higher temperature. However, the reduction peaks shifted to higher temperatures, which implying the redox activities of the catalysts were reduced by the amount of doped titanium. The H_2-TPR results showed that Mn/Ti(10)SNT had the largest area for the reduction peak of all catalysts, *i.e.*, it had the strongest redox and oxygen storage capacity. This was consistent with the results of the catalytic activity testing.

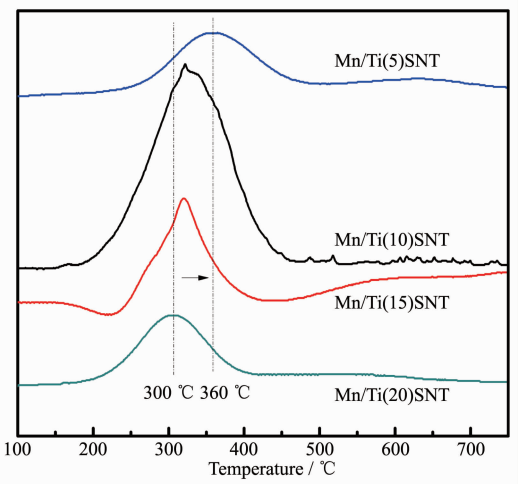

Fig.9 H_2-TPR curves of Mn/TiSNT catalysts with different Si/Ti molar ratios

3 Conclusions

Ti-containing SNT (TiSNT) with different Si/Ti molar ratios had been synthesized via a sol-gel and co-condensation method. When the Si/Ti molar ratio was more than 5, a hollow tubular morphology was clearly observed. When the Si/Ti molar ratio was located at 5 (Ti(5)SNT), the hollow morphology of Ti(5)SNT is destroyed. The Mn/TiSNT catalysts with

different Si/Ti molar ratios were prepared via an impregnation method. Their performances for SCR treatment of NO_x with NH_3 were evaluated. Among the Mn/TiSNT catalysts prepared, the Mn/Ti(10)SNT catalyst was the best for SCR of NO. The results indicate that over 90% of NO conversion was achieved at a low temperature of 135 ℃. Meanwhile, the NO conversion rate remained larger than 90% from 135 to 325 ℃. When the Si/Ti molar ratio was more than 5, the catalyst had a large specific surface area indicating that it could provide a high active surface. XPS results show that the surface-adsorbed oxygen of the Mn/Ti (10)SNT catalyst was the highest, which was favorable for SCR reaction. The TPR studies show that the Mn/Ti(10)SNT catalyst had the strongest redox capability and huge oxygen storage capacity. In addition, the superior activity is ascribed to the abundant acidic sites in Mn/Ti(10)SNT catalysts, which will promote the adsorption and activation of NH_3 on the surface of the catalysts.

Acknowledgments: The project was supported by the National Natural Science Foundation of China (Grants No. 21571024, 21101017/B0107), the Natural Science Foudnation of Jiangsu Province (Grant No.BK20181056), the Colleges and Universities in Jiangsu Province Plans to Graduate Research and Innovation (Grant No.SJZZ15_0142) and State Key Laboratory of Coordination Chemistry (Grant No.SKLCC1802).

References:

[1] Kapar J, Fornasiero P, Hickey N. *Catal. Today*, **2003**,**77**:419-449

[2] Nowak R. *Science*, **1994**,**263**:1217-1219

[3] Fedeyko J M, Chen B, Chen H Y. *Catal. Today*, **2010**,**151**:231-236

[4] Nedyalkova R, Shwan S, Skoglundh M, et al. *Appl. Catal. B*, **2013**,**138**:373-380

[5] Wang L S, Huang B C, Su Y X, et al. *Chem. Eng. J.*, **2012**, **192**:232-241

[6] Lou X R, Liu P F, Li J, et al. *Appl. Surf. Sci.*, **2014**,**307**:382-387

[7] Yu C L, Chen F, Dong L F, et al. *Environ. Sci. Pollut. Res.*, **2017**,**24**:7499-7510

[8] Wang X B, Wu S G, Zou W X, et al. *Chin. J. Catal.*, **2016**, **37**:1314-1323

[9] Boukha Z, De La Torre U, Pereda-Ayo B, et al. *Top. Catal.*, **2016**,**59**:1002-1007

[10]Xie G Y, Liu Z Y, Zhu Z P. *J. Catal.*, **2004**,**224**:42-49

[11]Jiang X, Lu P, Li C T, et al. *Environ. Technol.*, **2013**,**34**:591-598

[12]Long R Q, Yan R T. *J. Catal.*, **2002**,**207**:158-165

[13]Chen L H, Li X Y, Tian G, et al. *Angew. Chem. Int. Ed.*, **2011**,**50**:11156-11161

[14]Ko Y, Kim S J, Kim M H, et al. *Microporous Mesoporous Mater.*, **1999**,**30**:213-218

[15]Li L D, Wu P, Yu Q, et al. *Appl. Catal. B*, **2010**,**94**:254-262

[16]Ye Y Z, Shen F, Wang H N, et al. *J. Chem. Sci.*, **2017**,**129**:765-774

[17]Charbonneau L, Kaliaguine S. *Appl. Catal. A*, **2017**,**533**:1-8

[18]Zhang W Z, Frba M, Wang J L, et al. *J. Am. Chem. Soc.*, **1996**,**118**:9164-9171

[19]Marchese L, Maschmeyer T, Gianotti E, et al. *J. Phys. Chem. B*, **1997**,**101**:8836-8838

[20]Shen B X, Zhang X P, Ma H Q, et al. *J. Environ. Sci.*, **2013**, **25**:791-800

[21]Qi G S, Yang R T. *J. Phys. Chem. B*, **2004**,**108**:15738-15747

[22]Qu Y F, Guo J X, Chu Y H, et al. *Appl. Surf. Sci.*, **2013**, **282**:425-431

[23]Hou S C, Cao Y, Xiong W, et al. *Ind. Eng. Chem. Res.*, **2006**,**45**:7077-7083

[24]Wu Z B, Jin R B, Liu Y, et al. *Catal. Commun.*, **2008**,**9**:2217-2220

[25]Jampaiah D, Tur K M, Venkataswamy P, et al. *RSC Adv.*, **2015**,**5**:30331-30341

[26]Rivallan M, Ricchiardi G, Bordiga S, et al. *J. Catal.*, **2009**, **264**:104-116

[27]Martins G V A, Berlier G, Bisio C, et al. *J. Phys. Chem. C*, **2008**,**112**:7193-7200

[28]Kuehl G H, Timken H K C. *Microporous Mesoporous Mater.*, **2000**,**35**:521-532

[29]Dwyer J. *Stud. Surf. Sci. Catal.*, **1988**,**37**:333-354

[30]Gac W. *Appl. Catal. B*, **2007**,**75**:107-117

[31]Lv G, Bin F, Song C L, et al. *Fuel*, **2013**,**107**:217-224